# Automated Detection and Location of Tectonic Tremor along the Entire Cascadia Margin From 2005-2011

Boyarko, D. C. (1), Brudzinski, M. R. (1), Porritt, R. W. (2), Allen, R. M. (2), Tréhu, A. M. (3)

(1) Miami University, Department of Geology and Environmental Earth Science, Oxford, OH, USA.
(2) University of California, Berkeley, Department of Earth and Planetary Science, Berkeley, CA, USA.
(3) Oregon State University, College of Earth, Ocean, and Atmospheric Sciences, Corvallis, OR, USA.

## Abstract

We have constructed an automated routine to identify prominent bursts of tectonic tremor and locate their source region during time periods of raised amplitude in the tremor passband. This approach characterizes 62 episodes of tectonic tremor between 2005 and 2011, with tremor epicenters forming a narrow band spanning the entire length of the Cascadia Subduction Zone. We find a range of along-strike lengths in individual episodes, but the length appears proportional to both duration and geodetic moment, consistent with proposed scaling laws for slow earthquake phenomena. Examination of individual episodes in detail reveals intriguing updip-downdip migration patterns, including slow updip migration during initiation and repetitive downdip migration between different episodes. The broader catalog of tremor episodes refines the inferences from earlier work that episodic tremor and slip is segmented along-strike and correlated with apparent seismogenic zone segmentation based on the distribution of fore-arc basins and geologic terranes. The overall band of tremor is offset ~50 km from the downdip edge of interseismic coupling along the central and northern parts of the subduction zone. Along the southern part of the

subduction zone, it is adjacent to this boundary, suggesting that the locked and transition zones may be more closely linked in southern Cascadia.

**1. Introduction**

In subduction zones, changes in interplate coupling along the megathrust result in changes in the style of slip with increasing depth on the subduction interface. Locking along the shallow seismogenic zone results in infrequent large interplate earthquakes, while aseismic stable sliding occurs along the deeper portion due to changing material properties. The transition zone between these end-member styles of interplate slip appears to be more complicated than simple stick-slip behavior. The factors responsible for the transition in slip behavior from the seismogenic zone to the stable slip zone remain in dispute, and accurate, precise information on to the location of the transition zone may have significant implications for estimates of the region of the subduction interface capable of radiating seismic energy and causing strong shaking in a great earthquake.

Advances in seismic and geodetic monitoring systems have led to the discovery of a unique class of slow earthquakes, including episodic tremor and slip (ETS) originating from the transition zone of the subduction interface [e.g., Beroza and Ide, 2011]. Surface-based geodetic instruments provide clear evidence of recurring episodes of transient slip with durations of days to weeks, which show ground motions opposite to the direction of relative plate convergence [Dragert et al., 2001]. Often associated with these episodes of transient slip is an emergent, extended-duration, seismic signal resembling an intense swarm of microseismicity with overlapping seismic waves deficient in higher frequency energy, which is generally referred to as tectonic tremor [Rogers and Dragert, 2003]. The close spatial and temporal coincidence of tectonic tremor and transient slip, observed in several subduction zones, suggests these two phenomena are different manifestations of a common source process [e.g., Schwartz and Rokosky, 2007].

In comparison to traditional earthquakes, subduction zone tremor is a relatively low amplitude seismic signal that is quasi-continuous during a transient slip episode [Obara, 2002]. Constraining precise tremor source locations is often challenging due to the lack of impulsive body wave arrivals used in traditional earthquake location techniques. Consequently, many previous studies have employed envelope waveform cross correlation techniques which yield optimized time lags used to resolve source locations with reliable horizontal uncertainties, but less certain vertical uncertainties [Obara, 2002; Payero et al., 2008; Wech and Creager, 2008].

Tectonic tremor has been particularly difficult to locate in portions of Cascadia with large station spacing and irregular distribution of seismic instruments. Studies concentrating on the seismic component of tremor and slip have been focused toward the northern end of the subduction zone due to the higher density of seismic instruments [e.g., Kao et al., 2009; Wech et al., 2009; Houston et al., 2011], while the rest of the margin has received considerably less attention [e.g., Szeliga et al., 2004; Boyarko and Brudzinski, 2010; Bartlow et al., 2011]. In northern Cascadia, several studies have documented the remarkable temporal and spatial correlation between tectonic tremor and transient slip [Kao et al., 2009; Wech et al., 2009], indicating that the overall distribution of tectonic tremor matches the inferred distribution of transient slip. This correlation is particularly well documented for episodes that migrate through a 200-300 km segment of the subduction interface in northern Washington, repeating on average every 14 ± 1 months [e.g. Rogers and Dragert, 2003; Brudzinski and Allen, 2007; Wech et al., 2009]. In fact, comparisons of different episodes reveal some common migration patterns [Houston et al., 2011].

Outside of the northern Washington segment, correlations between transient offsets in GPS time series and raised amplitudes in the tremor passband suggest that ETS occurs throughout the subduction zone despite the relatively sparse seismic and GPS station spacing [Brudzinski and Allen, 2007; Holtkamp and Brudzinski, 2010]. ETS in these other regions does not repeat as regularly in time, with standard deviations 2-5 times larger than for the northern Washington segment [Brudzinski and Allen, 2007].

Moreover, tremor source location analysis in other parts of the subduction zone has been limited [Boyarko and Brudzinski, 2010; Bartlow et al., 2011; Ide, 2012], resulting in uncertainty about whether patterns observed in the northern Washington region are characteristic of the entire subduction zone or whether they reflect anomalous behavior where the subducting plate must accommodate a unique bend due to a ~45° change in the strike of the trench.

To increase our understanding of tectonic tremor and transient slip phenomena, we conducted a comprehensive analysis of tectonic tremor episodes spanning the entirety of the Cascadia Subduction Zone. This analysis reveals several unique modes of simple and complex migration with components of migration parallel and normal to the strike of the subducting plate. The tremor source region appears to be divided into several distinct segments along-strike based on the lateral extent, epicenter density, and recurrence interval of tremor episodes. Comparison of the distribution of tremor with the predicted plate interface depth, thermal structure, and interseismic coupling helps to delineate the physical conditions of the frictional transition zone.

## 2. Data and Methods

We present a catalog of prominent tectonic tremor activity between 2005 and 2011 constructed by applying a newly designed automated location routine to seismic data spanning the entire length of the Cascadia subduction zone (Figure 1). The framework of the automated tremor location routine is derived from a previously developed semi-automated location routine [Boyarko and Brudzinski, 2010]. The semin-automated approach focused on time periods of elevated tectonic tremor energy [Brudzinski and Allen, 2007], identified the most pronounced signals on stacked envelope seismograms, and inverted analyst-refined arrival times for source locations. The automated location routine incorporates two additional components: the definition of evenly spaced network subsets to aid in detection of concurrent tremor at different locations along strike and a cross correlation procedure to identify waveform similarity and perform arrival time refinement. Together, these additional components facilitate a more objective means of identifying and locating tectonic tremor, although the technique remains biased towards the larger bursts of tremor energy. This procedure is computationally efficient and readily applicable to permanent and temporary seismic networks, allowing us to expand the scope of the previous semi-automated analysis both spatially and temporally.

The seismic data used in this study come from the permanent and temporary networks of the Berkeley Digital Seismic Network (BDSN), Cascadia Arrays for EarthScope (CAFE), Canadian National Seismograph Network (CNSN), Central Oregon Locked Zone Array (COLZA), Flex-array Along Cascadia Experiment for Segmentation (FACES), Global Seismographic Network (GSN), Oregon Array for Teleseismic Study (OATS), Pacific Northwest Seismic Network (PNSN), Plate Boundary Observatory (PBO), Portable Observatories for Lithospheric Analysis and Research Investigating Seismicity (POLARIS), and the Transportable Array (TA). Figure 1 illustrates how the temporary networks helped to increase the station density in underserved areas of the margin. We remove the instrument response and filter to a narrow tremor passband to normalize the recordings across different seismic networks.

**2.1 Tremor Episode Detection**

We focus our analysis on time periods of elevated tectonic tremor activity using a master network of stations with high tremor signal-to-noise ratios. All waveform analysis in this study begins by removing the instrument response from hour-long seismograms, applying a bandpass filter from 1-6 Hz, and calculating the envelope. Tremor activity is calculated from the mean amplitude of filtered envelope seismograms recorded at individual stations, excluding hours with evidence of earthquakes, cultural noise, or instrument problems. Following the application of a four-day moving average and normalizing each time series, peaks above the background noise at 99% confidence are identified as major time periods of vigorous tectonic tremor. In addition, time periods of minor tectonic tremor are observed which do not clearly rise above the background noise, but which still exhibit coherent amplitudes at several neighboring stations, suggesting a tectonic source. These time periods of major and minor tremor activity constitute the focus of our investigation into the spatial and temporal record of tectonic tremor.

**2.2 Subdivision of the Seismic Network**

It is well documented that multiple regions can concurrently experience elevated levels of tectonic tremor [Kao et al., 2009; Boyarko and Brudzinski, 2010]. To minimize the potential for signal interference between two or more competing source regions, the Cascadia Subduction Zone is subdivided into eleven subnetworks. Each subnetwork is centered on a degree of latitude and extends one degree to the north and to the south, providing partial overlap by one degree. Within each subnetwork, one hour long envelope seismograms are correlated between each station pair. Stations are removed if their average correlation coefficient with respect to the other stations within the regional network is greater than 1 standard deviation from the average correlation coefficient of the entire regional network. Furthermore, only source locations within ±0.5° from the center of each region are retained, which ensures good azimuthal coverage of the tremor wavefield and decreases the potential for duplicate locations among neighboring regions.

**2.3 Individual Tremor Burst Identification and Source Location**

The signal processing component of the automated source location routine starts with the same envelope seismograms produced during the tremor detection procedure. To further enhance coherent tremor signals from station to station relative to the background noise, a 0.06 Hz low-pass filter is applied. We stack multicomponent envelope waveforms at a given site to reduce noise when looking for station to station correlations [Boyarko and Brudzinski, 2010], which also facilitates the use of vertical component data in conjunction with three component data.

A key difference between our approach and that of others [Obara, 2002; Wech and Creager, 2008] is that we optimize processing by only focusing on times of prominent tremor bursts, whereas previous studies have sought to analyze all available time windows. To identify the most prominent tremor signals across the network, a composite network time series is generated by stacking the envelope time series of each station encompassed within a given network subset. The remaining signals rising above the background noise with an amplitude ratio over a short-term window (10 s) and long-term window (100 s) that is greater than 2 are considered to be tectonic in origin. For detections in the composite network time series, the maximum amplitude signal within 15 seconds in each individual stacked envelope time series is identified and treated as apparent S wave arrival. To evaluate waveform similarity and perform arrival time refinement, a 100 second time window around each set of arrivals is cross correlated. The resulting sets of arrivals, if observed at a minimum of four stations, are used as input into a grid searching algorithm that solves for the source location that minimizes travel time residuals [Hermann, 2004]. In addition to source location errors obtained from the grid searching algorithm, the horizontal source location error is estimated using a bootstrap reliability test [Efron, 1979; Wech and Creager, 2008; Boyarko and Brudzinski, 2010].

**2.4 Catalog Refinement**

To produce a spatially and temporally coherent tectonic tremor catalog, the initial catalog generated from our processing is refined with the application of culling and clustering procedures, consistent with approaches outlined in earlier studies [Wech and Creager, 2008; Boyarko and Brudzinski, 2010]. In the culling procedure, solutions with significant position and correlation errors are removed such that only sources with errors less than 10 km in all directions and correlation coefficients greater than 0.65 are retained. In the clustering procedure, each solution is required to occur in the presence of a minimum of two additional solutions inside a 0.3 × 0.3 degree area and 3 day time frame to be included in the final catalog. In effect, these two procedures assist in removing singular seismic sources such as earthquakes and provide a more reliable spatial and temporal assessment of a persistent, migrating source.

## 2.5 Validation By Comparison with Previous Results

To provide a sense of the accuracy of our automated location routine, source location results obtained from similar data sets along the southern half of the subduction zone using semi-automated and automated location routines are compared (Figure S1). The automated location routine produces similar spatial and temporal trends as the semi-automated location routine, with the exception of a small episode (E5 in January 2006) in which tremor sources were only identified through careful examination of envelope waveforms due to limited station coverage during that period of time [Boyarko and Brudzinski, 2010]. The automated location routine improves the resolution of tremor including the identification of additional source regions and a tighter concentration of tremor sources that reveal more details of tremor migration in the strike direction. The reproducibility and improved resolution of these tremor episodes attest to the capability of the automated location routine to detect and locate tremor source locations over large spatial and temporal scales.

## 3. Seismic Processing Results

The application of our processing to seismic data from 2005-2011 resulted in the identification of over 10,600 tremor locations that span the length of the subduction zone and concentrate in a narrow region that roughly follows the strike of the subducting plate (Figure 1). The spatial and temporal distribution of tremor along the subduction zone is shown in Figure 2. In this reference frame, the clusters of tremor locations extending in the strike direction advance at slow rates (km/d) and endure for extended periods of time (days to weeks), in contrast to the fast rates (km/s) and short time scales (seconds to minutes) associated with ordinary earthquake ruptures.

### 3.1. Spatial Extent and Temporal Duration of Tremor Episodes

We define an episode of tectonic tremor to be a group of spatially and temporally coherent tremor solutions by requiring that a minimum of 20 solutions occur in the presence of an additional solution inside a 0.3 × 0.3 degree area and 3 day time frame. The requirement for repeating source locations follows the fundamental definition used in previous studies that tremor is an enduring correlated signal localized in space [Obara, 2002; Wech and Creager, 2008]. Application of this operation to data from 2005-2011 resulted in the identification of 62 tremor episodes, each of which is assigned an alphanumeric character (E1, E2, E3, etc.) that increases in value according to the start date of the episode (Table S1).

Source parameters including length, duration, migration rate, and directionality are estimated to measure the extent and growth of each episode (Table S1). Durations are calculated by summing the number of active tremor days in a given episode. Lengths are calculated by measuring the distance separating the mean position of the five most extreme tremor solutions in the strike direction such that the effects of outliers along the edges of a given episode are minimized.

The strike-parallel length of a tremor episode is proportional to its duration as shown in Figure 3. Such a relationship between length and duration is consistent with migration rates reported in earlier studies [Kao et al., 2009]. Slow slip phenomena have seismic moment proportional to duration while traditional earthquakes have moment proportional to duration cubed [Ide et al., 2007; Aguiar et al., 2009] and this suggests that the seismic moment in Cascadia, and elsewhere, is controlled primarily by how far an individual event extends along-strike.

**3.2 Strike-Parallel Migration Rates and Directionality**

The migration of tremor parallel to the strike of the subducting plate is a common feature observed in many episodes of tectonic tremor [Obara, 2002; Kao et al., 2009; Wech et al., 2009; Boyarko and Brudzinski, 2010; Houston et al., 2011]. In previous studies, the spatial and temporal evolution of tectonic tremor episodes have typically been characterized by unilateral or bilateral sequences that migrate along the strike of the subduction zone at rates on the order of ~10 km/day [Kao et al., 2009; Boyarko and Brudzinski, 2010]. In addition, there are accounts of more complex strike-parallel migration patterns including temporally-continuous, but spatially-discontinuous, along-strike migration of multiple source regions and terminating fronts of migrating tremor following convergence into recently active regions [Kao et al., 2006; Boyarko and Brudzinski, 2010].

By analyzing tremor along the entire Cascadia margin over a 5-year time span, we identify systematic trends in the spatial extent, temporal duration, migration rates and directionality, tremor initiation and termination. In particular, we focus on observations of strike-parallel and strike-normal tremor migration for episodes shown in Figure 2. Relative to the tremor centroid line (Figure 1), negative strike-normal positions occur on the updip half of the tremor source region, and positive strike-normal positions occur on the downdip half of the tremor source region.

Migration rates are calculated by linear regression applied to the spatial and temporal positions of tremor solutions exhibiting steady motion, with positive migration defined to be to the north or updip. In our catalog of tremor episodes, at least 6 episodes exhibit considerable variability in strike-parallel migration rates and directions during the course of a given episode. In these cases, episodes are separated into multiple groups of locations, requiring each sub-episode having at least five days of continuous tremor. For the following analysis, we only consider linear regressions with a correlation coefficient greater than 0.8 to be meaningful.

Approximately 50% of the episodes in our catalog exhibit clustering of tremor solutions sufficient to resolve strike-parallel migration rates. The results indicate tremor advances at rates ranging from 3-16 km/d, with a margin-wide average migration rate of 8.7 km/d, consistent with the 8.3 km/d scaling factor relating the length and duration source parameters (Figure 3). There is a slight indication of regional variability in tremor migration rates with mean values of 8.9 km/d, 7.0 km/d and 9.5 km/d in the southern, central, and northern regions of the subduction zone, although the sample size in these regions is small enough that the standard deviations overlap.

There appear to be no subduction-zone-wide trends in the directionality of strike-parallel migration. Previous work suggested the existence of a preferred migration direction for one segment in northern Washington [Houston et al., 2011]. We also find 5 tremor episodes (E2, E16, E36, E45, E58) that migrated several hundred kilometers from south to north across this segment (S6) over periods of about 5 weeks. However, none of the other segments show a preferential migration direction. Overall, we find 16 episodes that migrate to the north and 14 that migrate south (Table S1).

**3.3 Tremor Initiation**

In a recent study of northern Washington tremor episodes, many episodes appear to initiate along deeper parts of the tremor source region and expand to shallower parts of the fault prior to migrating northward [Wech and Creager, 2011]. This study also found that durations of tremor episodes and recurrence intervals between them were gradually shorter with increasing depth, which was likewise found in Japan [Obara et al.,2012]. The deep-to-shallow migration patterns and depth-duration-recurrence relationships were interpreted with a deterministic stress transfer model [Wech and Creager, 2011], where the fault is progressively stronger in the updip direction, such that each tremor and slip adds stress to the region immediately updip from it until it reaches the higher yield stress, promoting updip migration. Stable sliding below the ETS zone is thought to produce the stress that trigger the deepest tremor, which is presumably the weakest part of the fault based on the shortest recurrence times. A global comparison of ETS recurrence intervals with fore-arc velocity structure suggests that silica enrichment may be responsible for the weakening and shorter recurrence times [Audet and Bürgmann, 2014].

To examine if tremor is prone to initiating along the base of the tremor source region and migrating upward, we analyzed the initiation phase of tremor episodes in our catalog across the entire subduction zone. Strike-normal centroid curves for each episode of sufficient length are approximated by calculating the mean strike-normal position over a ±2 day time frame (Figure 4). Analysis of the regularly recurring episodes along the northern end of the margin (E2, E16, E36, E45) complements the results presented in earlier studies [Houston et al., 2011; Wech and Creager, 2011], as the majority of these episodes initiate in the downdip half of the tremor source region and exhibit an updip progression prior to switching to mostly strike-parallel migration (Figure 5a). However, our catalog reveals that one of these episodes (E36) shows evidence for originating updip before quickly migrating downdip and then following an updip migration pattern similar to episode E45.

The majority of episodes in our catalog exhibit an updip migration during the first week of an episode (Figure 4). However, closer examination of our catalog reveals that not all episodes initiate along the downdip end of the tremor source region (Figure 4c). Even if we include the events in Northern Cascadia that primarily initiate on the downdip end, the majority of tremor episodes tend to initiate within ±5 km of the center of the tremor source region and stay within 10 km of the tremor centroid through the course of the first week of activity (Figure 4b). This indicates that initiation in Central and Southern Cascadia does not generally follow the deterministic stress transfer model where episodes are primarily driven by stable sliding below the ETS zone. It is not clear what causes this difference, but if the stress transfer is more deterministic in the Puget Sound region, it may help explain why the recurrence intervals are more regular than in other regions [Brudzinski and Allen, 2007].

### 3.4 Repeating Episodes of Complex Tremor Evolution

In this section, the detailed migration patterns of several episodes are discussed to draw attention to two key findings about tremor evolution: (1) superimposed on variable rates of strike-parallel tremor migration are variable rates of strike-normal migration, and (2) several segments along the margin show remarkably similar patterns of tremor migration between different episodes.

The first example of these findings can be seen in the northern Washington region (Figure 5a), which has been examined in previous studies [Wech et al., 2009; Houston et al., 2011]. Episodes E36 and E45 in May 2008 and 2009, respectively, occur over similar spatial and temporal scales, with source durations that span several weeks and lengths that exceed 250 km in the strike direction. During the early stage of these episodes, tremor migrated 10-20 km updip over the course of a week and then advanced mostly parallel to the strike of the tremor source region for a period of 10-14 days. This strike-parallel migration was followed by an intriguing downdip excursion over a period of 5-9 days that occurred in a similar location beneath southern Vancouver Island. The downdip excursions coincide with a distinct decrease in the strike-parallel migration rate. After the down-dip excursions, strike-parallel migration continued for 5-10 days, although the rate and distance in this final stage of tremor migration differed for the two episodes.

A second pair of "repeating tremor" episodes, E1 and E33, occurred in September 2005 and April 2008 across the southern end of the subduction zone (Figure 5b). In the early stage of these episodes, tremor initiated at the updip edge of the tremor source region and expanded downdip and slowly along strike over a period of 5-7 days. After this initiation phase, tremor advances more rapidly along strike and more gradually updip over a period of 13-18 days. A key aspect of this pair of episodes is that the initial downdip migration moved from near the 40 km contour of the subduction interface to the 50 km contour before changing direction and steadily migrating back to shallower slab depths. Older versions of the slab contours [McCrory et al., 2006] cause this migration patterns to appear to cut across several slab contours, so our tremor data favor the newer slab model [McCrory et al., 2012] and may suggest an even shallower dip near 41°N. Nevertheless, the sharp steepening of the slab at the southern edge in the new slab contours is consistent with the initial eastward migration we see in the tremor migration patterns.

A particularly intriguing pair of repeating tremor episodes, E11 and E26, in July 2006 and June 2007 overlap and extend north of the previously described pair of episodes. In contrast to the simple unidirectional migration characteristic of the pair to the south, this pair migrated bilaterally. Figure 5c illustrates the intriguing growth characteristics of these episodes, including a "delayed" bifurcation with activity in the southward-migrating track initiating approximately 6-8 days prior to the initiation of activity in the northward migrating track. This pattern is remarkable as typical bifurcation patternsexhibit initiation at the same position along strike and continuous growth outward along strike. The "delayed" bifurcation patterns are consistent for the two episodes, with tremor expanding to similar positions in the strike direction and similar migration rates in the southward and northward tremor fronts.

It is worth noting that these "repeating" episodes are not exact replicas of one another, as might be expected due to dynamic heterogeneity arising from complex slip histories in the time between episodes. However, these episodes all exhibit a similar point of initiation, similar trajectories with respect to the strike-normal migration of tremor, and similar migration rates. These observations of repeating tremor episodes argues for a specific set of conditions on the subduction interface conducive to generating these complex strike-parallel and strike-normal progressions. For example, the rare updip initiation and downdip migration in the southernmost episodes (Figure 5b) could reflect a feature related to being near the edge of the slab. Likewise, the remarkably similar locations of updip and downdip migrations in the northern episodes (Figure 5a) could be due to localized warping of plate interface structure associated with the broad bend in the slab, pushing tremor locations inland or seaward relative to a smoothed slab contour. The more complex delayed bifurcation pattern seen in the other pair of similar episodes is more difficult to explain. The spatial divergence is coincident with changes in the plate interface structure, but the cause of the delayed northward migration is unclear.

## 4. Comparisons with other Features of the Cascadia Subduction Zone

Geologic evidence in the form of turbidite and tsunami deposits indicate that great megathrust earthquakes have struck the Cascadia subduction zone with recurrence intervals ranging from 200-1200 years over the past 10,000 years [Nelson et al., 2006; Goldfinger et al., 2012]. The unusually small number of small and moderate-magnitude interplate earthquakes [Trehu et al., 2008; Williams et al., 2011] and complete absence of great earthquakes in modern times result in uncertainty about the structure of the seismogenic zone along the margin and, in particular, about the slip distribution on the plate boundary during large events. First order questions such as the area of the plate interface capable of generating substantial slip and possible along-strike variations in slip remain unanswered. Analysis of tectonic tremor provides information on the distribution of slip in the transition zone, which may offer new insights into the configuration of the adjacent, updip seismogenic zone.

**4.1 Recurrence Intervals**

The spatial and temporal records of tectonic tremor episodes reveal distinct regional changes in tremor recurrence, similar to trends established in earlier studies [Brudzinski and Allen, 2007; Holtkamp and Brudzinski, 2010], but with somewhat shorter recurrence intervals. We calculated the recurrence in 15 km x 15 km bins by taking the time between the first and last episode in each bin and dividing by one less than the total number of episodes with locations in that bin. Figure 6c shows the results for bins with at least 3 episodes. In southern Cascadia, we find two ~150-200 km wide patches that fill the two southernmost segments and recur on average every 6-8 months. In northern Cascadia, we find the ~300 km wide segment across the Puget sound shows two ~100 km patches of 8-12 month recurrence and the rest of the segment showing 12-16 month recurrence. In contrast to these other regions, central Cascadia has less frequent tremor episodes, but there is evidence from small patches for recurrence of 16-18 months in central Oregon and 20-24 months in northern Oregon and southern Washington . These results are consistent with previous estimates that tremor recurrence patterns can be grouped into three broad regions that correlate with geologic terranes (Klamath, Siletzia, and Wrangellia) [Brudzinski and Allen, 2007], which supports the idea that there are geologic controls that dictate the timing of tremor episodes.

In addition to these broad strike-parallel patterns of recurrence, we find evidence for strike-normal trends in recurrence as well. For example, the southern part of segment 6 across northern Washington shows a progressive decrease in recurrence interval from ~20 months at the updip end to ~6 months at the downdip end. This trend has been previously identified in a more detailed study focused on this segment [Wech and Creager, 2011] and in Nankai [Obara et al., 2012], with the former demonstrating that the trend we observe extends down to even smaller recurrence intervals at greater depths. We also observe a similar yet previously undocumented case of this trend in the central portion of segment 1 in northern California and segment 2 in southern Oregon, where the recurrence interval decreases from ~10 months at the updip end to ~2 months at the downdip end. This trend has been interpreted to represent an increasingly weaker interface with depth that leads to a lower failure threshold and shorter recurrence [Wech and Creager, 2011].

**4.2 Segmentation**

In our examination of the spatial and temporal trends of tectonic tremor, the observed patterns in tremor migration support the idea that the progression of spatially coherent migrating tremor is controlled by along-strike changes in the physical properties of the margin. For example, the nucleation and termination points of tremor episodes appear to recur at similar positions along strike (Figure 2), as noted in previous studies [Brudzinski and Allen, 2007; Boyarko and Brudzinski, 2010; Holtkamp and Brudzinski, 2010]. To quantitatively estimate which portions of the margin are most likely to be associated with the start and stop points of tremor episodes, we divided the margin into 30 km bins along strike and summed the number of times an episode began or ended in that bin. We weighted this sum by the number of tremor epicenters in each episode, such that more weight was given to larger episodes. Figure 6a shows the "segmentation factor" with darker red shading for larger weighted sums. These results are supported by the observation that regions with a relatively high "segmentation factor" coincide with pronounced minima in tremor density (Figures 2b and c).

Although the true nature of coseismic segmentation is unknown due to the lack of megathrust earthquakes in the historic record, segmentation of the megathrust has been inferred from geologic [Wells et al., 2003; Song and Simons, 2003] and paleoseismic [Goldfinger et al., 2012] evidence. Figures 6a and 6c shows locations of fore-arc gravity lows and sedimentary basins that are thought to be related to asperities on the plate interface [Wells et al., 2003], and Figure 6b shows apparent boundaries defined from the paleoseismic history [Goldfinger et al., 2012]. Tremor segmentation has been proposed to be correlated with the position of geologic terranes and forearc basins [Brudzinski and Allen, 2007] as well as the along-strike extent of prehistory earthquakes [Goldfinger et al., 2012].

In the following subsections, we attempt to integrate existing evidence for ETS segmentation in Cascadia with these other proxies for megathrust segmentation. Initial estimates of ETS segmentation were defined by the strike-parallel extent of larger episodes as seen on seismic and GPS instruments from 1998-2005 [Brudzinski and Allen, 2007]. Our current study provides more detailed tremor source locations along the entire margin and extends the catalog an additional 5 years. Moreover, we utilize additional observations along the margin including the tremor density, tremor recurrence, and tremor segmentation factor. Overall, we find evidence for 8 segments with lateral dimensions of 100-250 km (Figures 2 and 6). The strongest ETS evidence points to 3 fundamental segments that correspond to the terranes suggested by Brudzinski and Allen [2007], such that one might consider other boundaries to represent subsegments. In comparison to previous ETS segmentation estimates [Brudzinski and Allen, 2007], the spatial patterns of our tremor episodes complement the six initially proposed segment boundaries. In some cases, the along strike positions of our proposed segment boundaries are offset up to 50 km, which we attribute to the larger number of episodes and tremor epicenters upon which to base the segmentation model. In addition to these originally identified segment boundaries, our results support an additional segment boundary located at ~42°N. The location of this segment boundary corresponds with the reported 50 km wide minimum in tremor density inferred to represent an additional segment boundary [Boyarko and Brudzinski, 2010]. The following discussion is a systematic south to north description of the principal observations used to define each segment/subsegment and its boundaries.

**Klamath Terrane: Segments 1 and 2**

The southern end of the subduction zone is well defined by the southern termination of tremor activity (Figure 6a), which does not extend south of the Mendocino Triple Junction region despite the fact that our station coverage continues nearly 100 km further south (Figure 1). This termination appears to be the end of conditions under which tremor can occur as it is located ~50 km from the approximate southern edge of subducted lithosphere based on recent slab contours [McCrory et al., 2012] (Figure 1). However, seismic reflection surveys [Beaudoin et al., 1998] and joint inversions of surface waves with receiver functions indicate the southern edge is further north closer to the tremor epicenters [Liu et al., 2012] (Figure 1). Intriguingly, the edge of tremor locations progressively diverges from the apparent slab edge with increasing depth. We speculate that as subduction progresses, increasing penetration of heat into the slab or escape of fluids out of the slab along the southern edge could push the appropriate conditions for tremor further from the slab edge.

The northern termination of segment 2 is also marked by a high in segmentation factor and an abrupt decrease in tremor activity near 43°N (Figure 6). As noted previously [Brudzinski and Allen, 2007], this marks the boundary between more frequent tremor episodes with shorter recurrence intervals beneath the Klamath terrane and less frequent tremor episodes with longer recurrence intervals beneath Siletzia to the north. In addition to the onshore change in geologic terrane and topographic signature that support this segmentation boundary, there is paleoseismic evidence for 8 megathrust earthquakes that terminated just north of Rogue Apron (42.5°N), although half of those occurred over 6000 years before present and their extent is poorly constrained. Finally, the Cape Blanco headland (43°N), gap between the Coos Bay and Eel Bay basins, and edges of offshore gravity lows all indicate a boundary at or near this location.

The boundary between segments 1 and 2 can be characterized as a local lull in tremor activity rather than a consistent segment boundary. For example, repeating events E11 and E26 terminate about 75 km north of the southern edge of this region near 41°N (~150km along strike distance) and have a characteristic gap near 41.5°N

(~225km). The other pair of similar events in this region differs in their northern termination, E1 near 41.5°N and E33 near 42°N (~275km). Figure 2 shows that a variety of episodes that initiate or terminate at each of these potential subsegment boundaries (10 episodes near 150km, 8 episodes near 225 km, 4 episodes near 275 km). As a result, we see three peaks in segmentation factor (Figure 6a), reduction in tremor density between 41.5°N and 42°N [Boyarko and Brudzinski, 2010] (Figure 6b), and increased tremor recurrence between 41.5°N and 42°N (Figure 6c). We have chosen a compromise boundary at 42°N, in part because it corresponds to the approximate northern extent of two paleoseismic events (6b and 10e in Goldfinger et al. [2012]). There is additional support for subdivision of segment 1 based on both paleoseismic evidence [Valentine et al., 2012; Carver, 2000], the 1992 Petrolia earthquake [Tanioka et al., 1995], and a pair of offshore gravity lows (Figure 6), but this is contradicted by the broad Eel River Basin that matches the extent of segment 1.

**Siletzia Terrane: Segments 3, 4, and 5**

This region has the longest average recurrence interval and thus has the fewest episodes to interpret. The southern end of segment 3 and northern end of segment 5 occur at the approximate terrane boundaries and have the strongest segmentation factor in this region, but this is primarily due to tremor episodes from segments 2 and 6 terminating at these boundaries (Figures 2 and 6). There are only two episodes in segment 3 that terminate at the southern boundary.

The northern boundary of segment 3 is defined by 5 of 6 tremor episodes that terminate at this location, which produces an increase in segmentation factor at this boundary (Figures 2 and 6). The extent of segment 3 is matched by an offshore gravity low as well as the Coos Bay Basin. The available paleoseismic evidence is consistent with this extent but is less well resolved in this region. We also note that there appears to be an increase in recurrence intervals going north across this boundary from less than 20 months to greater than 20 months.

The boundary between segments 4 and 5 is not traversed by any of the 8 tremor episodes we identify in those segments, but there is only a brief pause between two episodes on either side of the boundary in late 2009. This results in a moderate increase in segmentation factor at the boundary. This boundary is correlated with a significant change in the thickness of the Siletz terrane [Trehu et al., 1995] and corresponding decrease in thickness of the upper plate rocks underlying Siletzia, which may be underplated oceanic crust and sediments and/or serpentinized upper mantle of the North American plate [Trehu et al., 1995; Bostock et al., 2002]. There is a broad offshore gravity low that traverses this boundary, with segment 4 correlated with the Newport and Astoria basins, while the extent of segment 5 correlated with the Willapa Basin. There are also 4 paleoseismic turbidites that terminate near the boundary between segments 4 and 5. Finally, the northern edge of segment 5 is defined by a strong segmentation factor, a large change in the thickness of the Siletz/Crescent terrane [Trehu et al., 1995; Wells et al., 1998], the edge of an offshore gravity low and sedimentary basin, but curiously little evidence for megathrust termination.

**Wrangellia Terrane: Segments 6, 7, and 8**

While lumped in with the Wrangellia terrane based on the prevalence in southern Vancouver Island [Jones et al., 1977], the southern portion of segment 6 is likely underlain by Crescent terrane that wraps around the Olympics [Trehu et al., 1995; Wells et al., 1998]. In any case, segment 6 is primarily defined by the well-recognized large tremor episodes that extend across the Puget Sound. Although the 5 large episodes show slightly variable northern and southern termination points on the order of 50 km, this is consistent with the uncertainties in the determination of along strike segmentation. The extent of segment 6 correlates with an offshore gravity low and Olympic Basin. Segment 8 is defined by 4 episodes that were best recorded during the POLARIS deployment on Northern Vancouver Island. Segment 7 is essentially the zone of weak tremor density first recognized as a persistent feature after a decade of tremor monitoring (1997-2007) [Kao et al., 2009]. Interestingly, the position of this gap occurs in close proximity to the landward projection of the Nootka Fault Zone and is coincident with the epicenters of two of the largest recorded crustal earthquakes in Vancouver Island [Kao et al., 2009]. This perhaps suggests the gap occurrence is related to a discontinuity in the subducting oceanic plates or a crustal stress anomaly associated with crustal seismicity.

**4.3 Interplate Coupling and Tectonic Tremor**

Finally, we compare the spatial distribution of tremor with the geodetic signature of the locked seismogenic zone of the plate interface. Establishing this relationship is important for addressing potential relationships between ETS and seismogenesis.

In Cascadia, the absence of historic great earthquakes and extremely low levels of interplate seismicity have prevented direct delineation of the seismogenic zone. Instead, thermal and geodetic estimates of interplate seismogenic potential have served as proxies for characterizing the dimensions of the seismogenic zone. Recent geodetic estimates of the downdip extent of interseismic coupling (Figure 1), which is based on long-term tidal and leveling records in southern Cascadia [Burgette et al., 2009] and time-dependent inversion of three-component continuous GPS in northern Cascadia [McCaffrey, 2009], provide a complex perspective of the structure of the locked and transition zones. Despite the different datasets, the two curves match within 10 km in the central part of the subduction zone where they overlap. The average distance between the downdip edge of interseismic coupling and the tremor source region varies along strike (Figure 1). The downdip edge of the geodetic transition zone abuts the tremor source zone in southern Cascadia but is offset by as much as 50 km in the northern half of the subduction zone.

It is important to underscore that in subduction zones where tectonic tremor and transient slip are both observed, there tends to be a gradation in the style of deformation with depth on the plate interface [Wang et al., 2008; Song et al., 2009; Wech et al., 2009; McCaffrey, 2009; Brudzinski et al., 2010]. For instance, in Washington the peak in the distribution of transient slip is typically offset 10-20 km updip from the peak in the distribution of tectonic tremor [Wech et al., 2009; Bartlow et al., 2011], whereas the two distributions show less separation in northern Oregon [Bartlow et al., 2011]. The offset of tremor and the downdip edge of interseismic coupling has serious implications for how one may interpret how ETS may impact the seismogenic zone.

Stress transfer between the seismogenic and transition zones is likely to be greatest in the regions where ETS is closest to the seismogenic zone. In fact, static stress modeling indicates the locked zone is brought closer to failure as a result of transient slip [Dragert et al., 2004]. As well, slow dynamic instabilities via transient slip could also conceivably accelerate, propagate updip, and evolve into an earthquake triggering mechanism [Matsuzawa et al., 2010].

Moreover, dynamic instabilities via megathrust earthquakes could continue to propagate down-dip into the ETS zone [Chapman and Melbourne, 2009]. This implies that coseismic slip could be accommodated as much as 50-100 km further inland than was previously thought. However, the spatially variable relationship between the locked zone, slow slip, and tremor suggest that potential triggering relationships are complex.

## 5. Conclusions

The application of our automated location routine to time periods of energetic tectonic tremor has resulted in the identification of over 10,000 tremor solutions that can be grouped into 62 episodes of tectonic tremor that exhibit spatial and temporal continuity. Tectonic tremor is concentrated in a narrow region spanning the entire length of the subduction zone. The along-strike length of a given tremor episode appears to increase as a function of duration, suggesting both length and duration are proportional to geodetic moment in Cascadia.

The detailed evolution of individual episodes of tectonic tremor exhibiting spatial and temporal continuity indicates several different modes of migration with components of motion parallel to and normal to the strike of the subducting plate. We find several cases of "repeating tremor" where an episode demonstrates migration patterns similar to those of earlier episodes, including changes in strike-parallel rates and strike-normal departures in similar locations. Previous studies of tremor evolution along northern Cascadia have shown tremor tends to initiate near the base of the tremor source region and expand updip in the first few days in these episodes. Although we find that tremor tends to expand updip in the first few days of an episode, tremor initiation occurs significantly down-dip of the tremor centroid line only in the Puget Sound region. Elsewhere, tremor initiates near the centroid line.

The tremor source region is found to be divided into several distinct segments based on the lateral extent, relative timing, and recurrence interval of tremor episodes. Two distinct segment boundaries correspond to the location of forearc terranes and reflect distinct changes in recurrence along the strike of the subduction zone. Other segment boundaries show some correlation with offshore gravity anomalies and forearc basins thought to represent long-term asperities and segmentation of the seismogenic zone. Others are correlated with differences in thickness of the upper crustal rocks within a forearc terrane, suggesting that there may be additional geologic boundaries near the base of the upper plate that control tremor characteristics.

The distribution of tectonic tremor is offset ~50 km from the downdip edge of interseismic coupling along the central and northern parts of the subduction zone, but is adjacent to the downdip edge of interseismic coupling along the southern part of the subduction zone. This suggests that if stress transfer occurs between the seismogenic and transition zones, then the southern end of the seismogenic zone is more likely to be influenced by ETS.

## 6. Acknowledgements

Support for this work was provided by NSF grants EAR-0847688 (MB), EAR-0643077 (RA), and EAR- 0550402 (AT). We relied heavily on data provided by the USGS, IRIS, Canadian, Pacific Northwest, Berkeley, and EarthScope Seismic Networks. We also thank those who contributed to EarthScope and POLARIS deployments in this region (FACES, COLZA, NVI, CAFE, and the Mendocino Experiment), which significantly improved the resolution of this study.

## 7. References

Aguiar, A. C., T. I. Melbourne, and C. W. Scrivner (2009), Moment release rate of Cascadia tremor constrained by GPS, J. Geophys. Res., 114, B00A05, doi:10.1029/2008JB005909.

Audet, P., and Bürgmann, R. (2014), Possible control of subduction zone slow-earthquake periodicity by silica enrichment, Nature, 510(7505), 389-392.

Bartlow, N. M., S. Miyazaki, A. M. Bradley, and P. Segall (2011), Space-time correlation of slip and tremor during the 2009 Cascadia slow slip event, Geophys. Res. Lett.,38, L18309, doi:10.1029/2011GL048714.

Beaudoin, B. C., J. A. Hole, and S. L. Klemperer (1998), Location of the southern edge of the Gorda slab and evidence for an adjacent asthenospheric window: Results from seismic profiling and gravity, J. Geophys, Res., 103(12), 30,101-30,115.

Beroza, G., and S. Ide (2011), Slow earthquakes and nonvolcanic tremor, Annu. Rev. Earth Planet. Sci., 39, doi:10.1146/annurev-earth-040809-152531.

Bostock, M. G., R. D. Hyndman, S. Rondenay, and S. M. Peacock (2002), An inverted continental Moho and serpentinization of the forearc mantle, Nature, 417, 536-538, doi:10.1038/4175361

Boyarko, D. C., and M. R. Brudzinski (2010), Spatial and temporal patterns of nonvolcanic tremor along the southern Cascadia subduction zone, J. Geophys. Res., 115, B00A22, doi:10.1029/2008JB006064.

Brudzinski, M. R., and R. M. Allen (2007), Segmentation in episodic tremor and slip all along Cascadia, Geology, 35, doi:10.1130/G23740A.1.

Brudzinski, M. R., H. R. Hinojosa-Prieto, K. M. Schlanser, E. Cabral-Cano, A. Arciniega-Ceballos, O. Diaz-Molina, and C. DeMets (2010), Nonvolcanic tremor along the Oaxaca segment of the Middle America subduction zone, J. Geophys. Res., 115, B00A23, doi:10.1029/2008JB006061.

Burgette, R. J., R. J. Weldon II, and D. A. Schmidt (2009), Interseismic uplift rates for western Oregon and along-strike variation in locking on the Cascadia subduction zone, J. Geophys. Res., 114, B01408, doi:10.1029/2008JB005679.

Carver, G.A., 2000, Paleoseismic geology of the southern part of the Cascadia subduction zone Penrose conference—Great Cascadia Earthquake Tricentennial Program summary and abstracts: Seaside, Oregon Department of Geology and Mineral Industries, p. 38–39.

Chapman, J. S., and Melbourne, T. I. (2009), Future Cascadia megathrust rupture delineated by episodic tremor and slip, Geophys. Res. Lett., 36, doi:10.1029/2009GL040465.

Dragert, H., K. Wang, and T. S. James (2001), A silent slip event on the deeper Cascadia subduction interface, Science, 292, doi:10.1126/science.1060152.

Dragert, H., K. Wang, and G. Rogers (2004), Geodetic and seismic signatures of episodic tremor and slip in the northern Cascadia subduction zone, Earth Planets Space, 56, 1143– 1150.

Efron, B. (1979), Bootstrap methods: Another look at the jackknife, Ann. Stat., 7, doi:10.1214/aos/1176344552.

Goldfinger, C., Nelson, C.H., Morey, A.E., Johnson, J.E., Patton, J.R., Karabanov, E., Gutiérrez-Pastor, J., Eriksson, A.T., Gràcia, E., Dunhill, G., Enkin, R.J., Dallimore, A., and Vallier, T. (2012), Turbidite event history—Methods and implications for Holocene paleoseismicity of the Cascadia subduction zone: U.S. Geological Survey Professional Paper 1661–F, 170 p. (Available at http://pubs.usgs.gov/pp/pp1661f/).

Hermann, R. B. (2004), Computer programs in seismology: Version 3.30, Saint Louis Univ., Saint Louis, Mo.

Holtkamp, S., and M. R. Brudzinski (2010), Determination of slow slip episodes and strain accumulation along the Cascadia margin, J. Geophys. Res., 115, B00A17, doi:10.1029/2008JB006058.

Houston, H., B. G. Delbridge, A. G. Wech, and K. C. Creager (2011), Rapid tremor reversals in Cascadia generated by a weakened plate interface, Nature Geoscience, 4, doi:10.1038/ngeo1157.

Hyndman, R. D., and K. Wang (1995), The rupture zone of Cascadia great earthquakes from current deformation and the thermal regime, J. Geophys. Res., 100, doi:10.1029/95JB01970.

Ide, S., G. C. Beroza, D. R. Shelly, and T. Uchide (2007), A scaling law for slow earthquakes, Nature, 447, doi:10.1038/nature05780.

Ide, S. (2012), Variety and spatial heterogeneity of tectonic tremor worldwide, J. Geophys. Res., 117, doi:10.1029/2011JB008840.

Jones, D.L., Silberling, N.J., and Hillhouse, J. (1977), Wrangellia; a displaced terrane in northwestern North America, Canadian Journal of Earth Sciences, 14, 2565–2577.

Kao, H., Shan, S. J., Dragert, H., Rogers, G., Cassidy, J. F., Wang, K. L., James, T. S., Ramachandran, K. (2006), Spatial-temporal patterns of seismic tremors in northern Cascadia, J. Geophys. Res., 111, doi:10.1029/2005JB003727.

Kao, H., S.-J. Shan, H. Dragert, and G. Rogers (2009), Northern Cascadia episodic tremor and slip: A decade of tremor observations from 1997 to 2007, J. Geophys. Res., 114, B00A12, doi:10.1029/2008JB006046.

Liu, K., Levander, A., Zhai, Y., Porritt, R. W., & Allen, R. M. (2012), Asthenospheric flow and lithospheric evolution near the Mendocino Triple Junction, Earth and Planetary Science Letters, 323-324, doi:10.1016/j.epsl.2012.01.020.

Matsuzawa, T., H. Hirose, B. Shibazaki, and K. Obara (2010), Modeling short- and long-term slow slip events in the seismic cycles of large subduction earthquakes, J. Geophys. Res., 115, B12301, doi:10.1029/2010JB007566.

McCaffrey, R. (2009), Time-dependent inversion of three-component continuous GPS for steady and transient sources in northern Cascadia, Geophys. Res. Lett., 36, L07304, doi:10.1029/2008GL036784.

McCrory, P. A., Blair, J. L., Oppenheimer, D. H., & Walter, S. R. (2006), Depth to the Juan de Fuca slab beneath the Cascadia subduction margin - A 3-D model for sorting earthquakes, U.S. Geological Survey Data Series, 91, http://pubs.usgs.gov/ds/91/.

McCrory, P. A., Blair, J. L., Waldhauser, F., & Oppenheimer, D. H. (2012), Juan de Fuca slab geometry and its relation to Wadati-Benioff zone seismicity, J. Geophys. Res., 117, doi:10.1029/2012JB009407.

Obara, K. (2002), Nonvolcanic deep tremor associated with subduction in southwest Japan, Science, 296, 1679–1681, doi:10.1126/science.1070378.

Obara, K., T. Matsuzawa, S. Tanaka, and T. Maeda (2012), Depth-dependent mode of tremor migration beneath Kii Peninsula, Nankai subduction zone, Geophys. Res. Lett., doi:10.1029/2012GL051420, in press.

Nelson, A. R., H. M. Kelsey, and R. C. Witter (2006), Great earthquakes of variable magnitude at the Cascadia subduction zone, Quaternary Research, 65, 354–365.

Payero, J. S., V. Kostoglodov, N. Shapiro, T. Mikumo, A. Iglesias, X. Perez-Campos, and R. W. Clayton (2008), Nonvolcanic tremor observed in the Mexican subduction zone, Geophys. Res. Lett., 35, L07305, doi:10.1029/2007GL032877.

Rogers, G. and H. Dragert (2003), Episodic tremor and slip on the Cascadia subduction zone: The chatter of silent slip, Science, 300, 1942-1943, doi:10.1126/science.1084783.

Schwartz, S. Y., and J. M. Rokosky (2007), Slow slip events and seismic tremor at circum-pacific subduction zones, Rev. Geophys., 45.

Song, T.-R. A., and M. Simons (2003), Large trench-parallel gravity variations predict seismogenic behavior in subduction zones, Science, 301, doi:10.1126/science.1085557.

Song, T.-R. A., D. V. Helmberger, M. R. Brudzinski, R. W. Clayton, P. Davis, X. Pérez-Campos, and S. K. Singh (2009), Subducting Slab Ultra-Slow Velocity Layer Coincident with Silent Earthquakes in Southern Mexico, Science, 324, 502-506, doi:10.1126/science.1167595.

Szeliga, W., Melbourne, T. I., Miller, M. M., & Santillan, V. M. (2004). Southern Cascadia episodic slow earthquakes. Geophys. Res. Lett., 31(16), L16602, doi:10.1029/2004GL020824.

Tanioka, Y., K. Satake, and L. Ruff (2010), Sesimotectonics of the April 25, 1992, Petrolia earthquake and the Mendocino triple junction region, Tectonics, 14(5), 1095-1103, doi:10.1029/95TC01975.

Trehu, A. M., G. Lin, E. Maxwell, and C. Goldfinger (1995), A seismic reflection profile across the Cascadia subduction zone offshore central Oregon: New constraints on methane distribution and crustal structure, J. Geophys. Res., 100(B8), 15,101-15,116.

Trehu, A. M., Braunmiller, J., & Nabelek, J. L. (2008), Probable low-angle thrust earthquakes on the Juan de Fuca - North America plate boundary, Geology, 36(2), 127–130.

Valentine, D. W., E. A. Keller, G. Carver, W.-H. Li, C. Manhart, and A. R. Simms (2012), Paleoseismicity of the Southern End of the Cascadia Subduction Zone, Northwestern California, Bulletin of the Seismological Society of America, 102(3), 1059-1078.

Wang, K., H. Dragert, H. Kao, and E. Roeloffs (2008), Characterizing an ‘‘uncharacteristic’’ ETS event in northern Cascadia, Geophys. Res. Lett., 35, L15303, doi:10.1029/2008GL034415.

Wech, A. G., and K. C. Creager (2008), Automated detection and location of Cascadia tremor, Geophys. Res. Lett., 35, L20302, doi:10.1029/2008GL035458.

Wech, A. G., K. C. Creager, and T. I. Melbourne (2009), Seismic and geodetic constraints on Cascadia slow slip, J. Geophys. Res., 114, B10316, doi:10.1029/2008JB006090.

Wech, A. G., and K. C. Creager (2011), A continuum of stress, strength and slip in the Cascadia subduction zone, Nature Geoscience, 4, doi:10.1038/ngeo1215.

Wells, R. E., C. S. Weaver, and R. J. Blakely (1998), Fore-arc migration in Cascadia and its neotectonic significance, Geology, 26(8), 758-762, doi:10.1130/0091-7613.

Wells, R. E., R. J. Blakely, Y. Sugiyama, D. W. Scholl, and P. A. Dinterman (2003), Basin-centered asperities in great subduction zone earthquakes: A link between slip, subsidence, and subduction erosion?, J. Geophys. Res., 108(B10), 2507, doi:10.1029/2002JB002072.

Williams, M. C., Tréhu, A. M., & Braunmiller, J. (2011), Seismicity at the Cascadia plate boundary beneath the Oregon continental shelf, Bulletin of the Seismological Society of America, 101, 940–950.

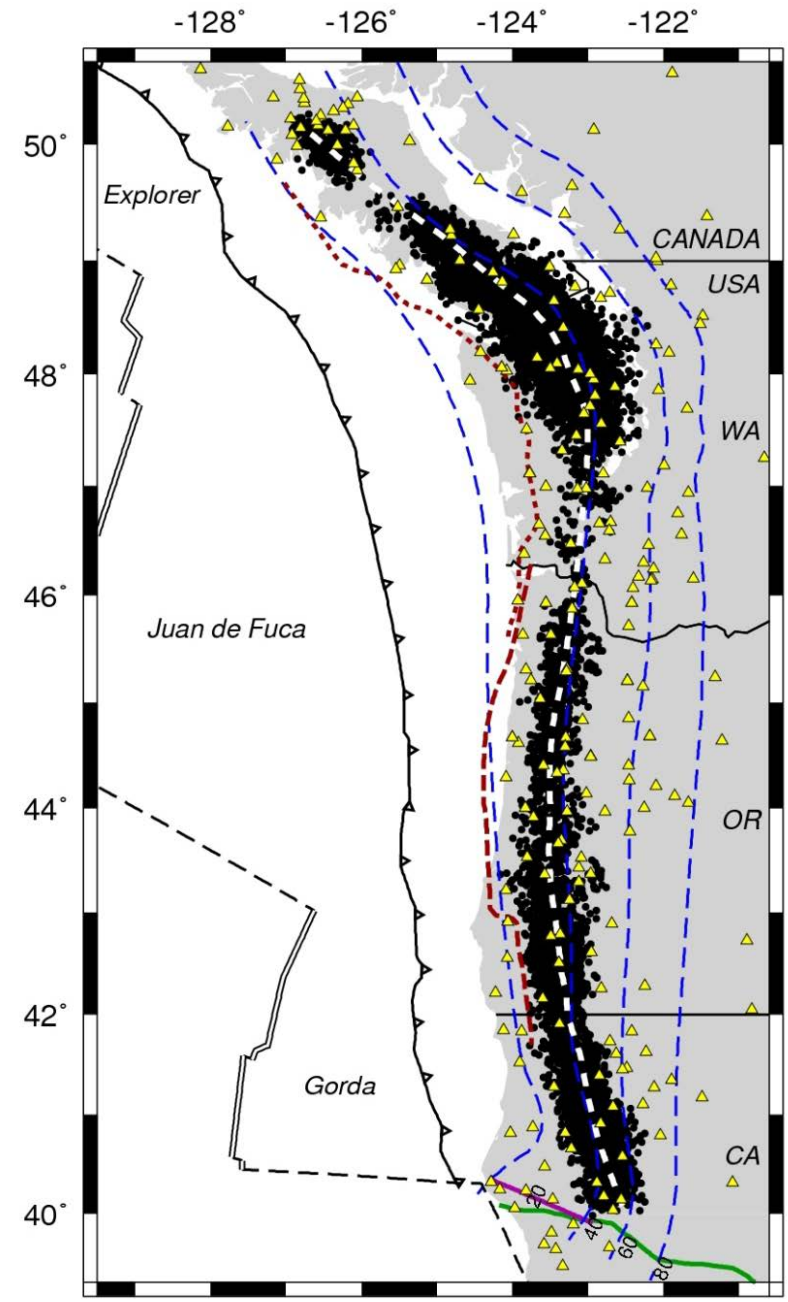


Figure 1. Map of tremor epicenters (black circles) along the Cascadia subduction zone, including plate boundaries, seismic stations used for this study (yellow triangles), and seismogenic zone inferred from estimates of interseismic coupling (dotted [McCaffrey, 2009] and dashed [Burgette et al., 2009]). Locations of tremor are from our analysis of episodes from 2005 and 2011. Some stations were active for only part of this period. White dashed line is centroid of tremor epicenters, defined by calculating the mean position of tremor solutions at regular intervals in the strike direction. Surface of the subducting plate (blue curves) is only shown to 80 km depth [McCrory et al., 2012]. Lines indicate southern edge of the subducting lithosphere based on Beaudoin et al. [1998] (purple) and Liu et al. [2012] (green).

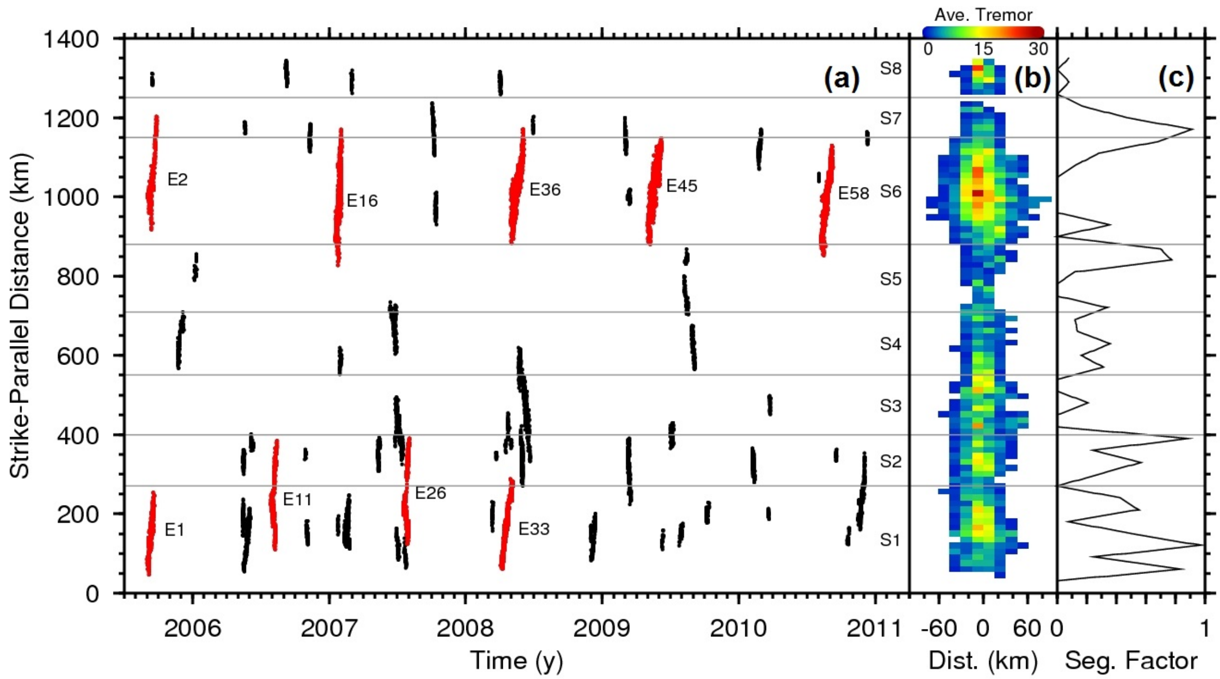


Figure 2. Spatial and temporal distribution of tremor solutions obtained from automated analysis of time periods with increased activity in the tremor passband. (a) Along strike distribution of tremor over time. Strike-parallel distance is measured along the centroid tremor source line (Fig. 1), where distance 0 represents 122.3W, 39.6N and 1400 is 127.74W, 50.66N. Thin gray lines are proposed segment boundaries of ETS. Labeled episodes are highlighted in red. (b) Tremor (NVT) density per episode. Density is based on gridding of all tremor epicenters into 20 km x 20 km bins, which is then divided by the number of episodes that produce epicenters in that bin. Plot shows the strike-normal distribution of tremor relative to the centroid tremor source line (Fig. 1), where negative is updip. (c) Smoothed segmentation factor, calculated from cumulative tremor episode sizes that initiated or terminated at that location.

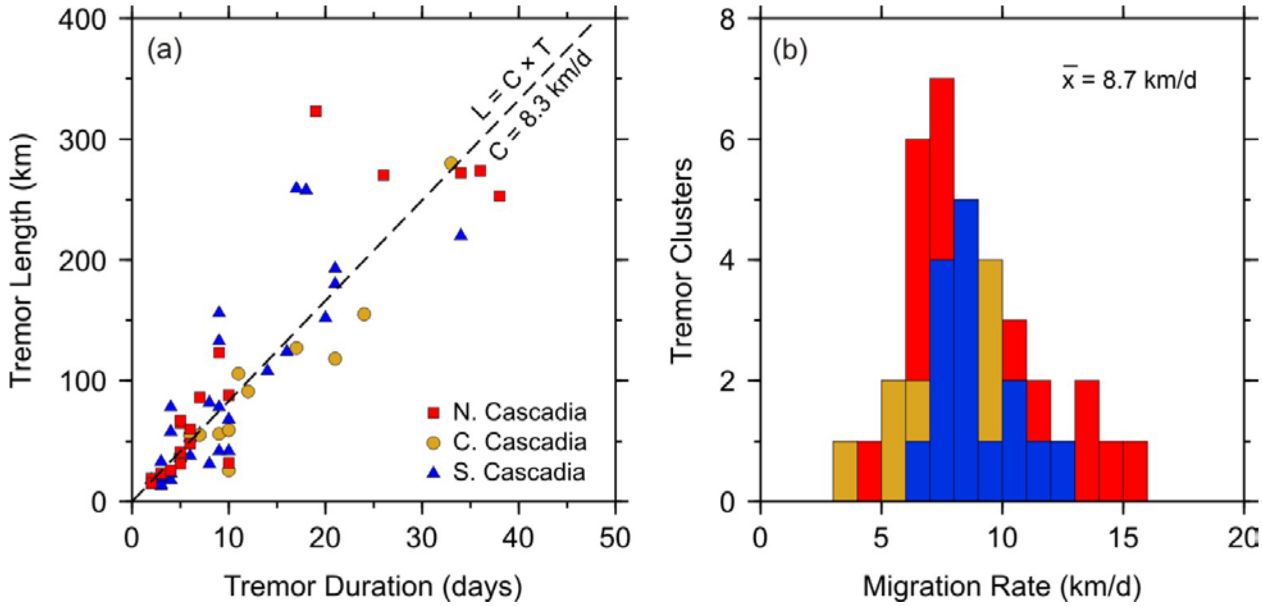


Figure 3. (a) Comparison of tremor length (L) measured in the strike direction and tremor duration (T) measured by summing the number of active tremor days. Velocity (C) regression curve (dashed line) is constrained within a 95% confidence interval to intersect the origin in order to satisfy physical requirements. Colors indicate area of the margin, where central Cascadia is defined as 43N to 46.5N. (b) Distribution of tremor migration rates based on spatially and temporally coherent clusters of tremor solutions with measurable migration. Colors indicate area of the margin.

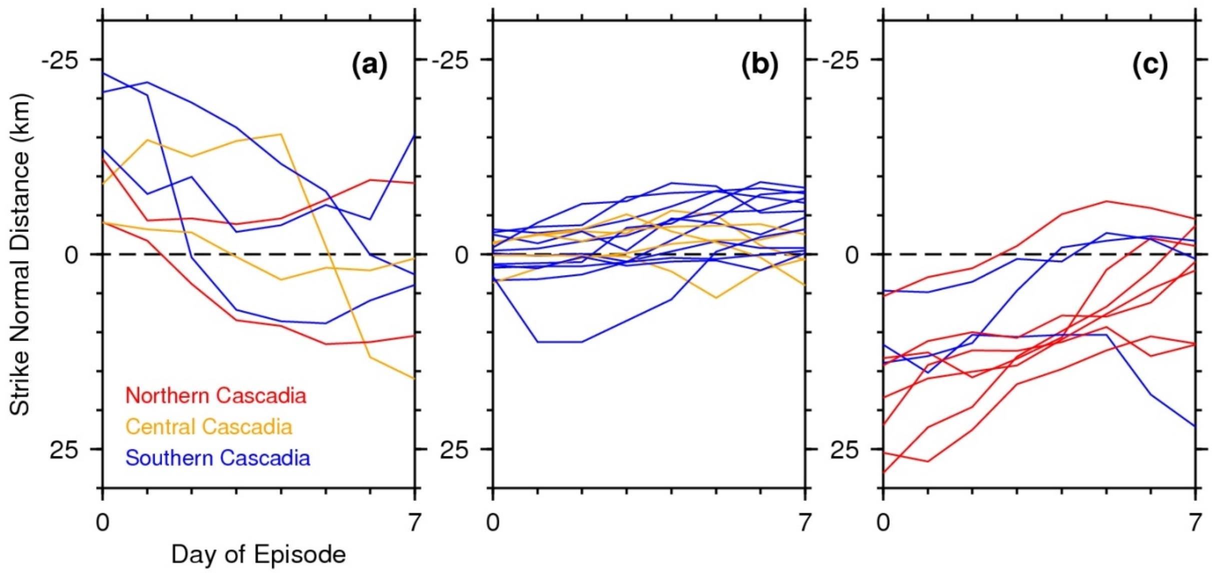


Figure 4. Tremor episode migration curves showing strike-normal locations relative to the overall tremor centroid (dashed line). Each point represents a four day moving average of epicenters in a given episode, where day 0 includes epicenters over the 2 days before and after the first epicenter. Episodes are separated based on whether they initiate along the (a) updip, (b) center, or (c) downdip sections. The majority of episodes initiate within 5 km of the centroid, and these show a 5-10 km updip migration over the first few days.

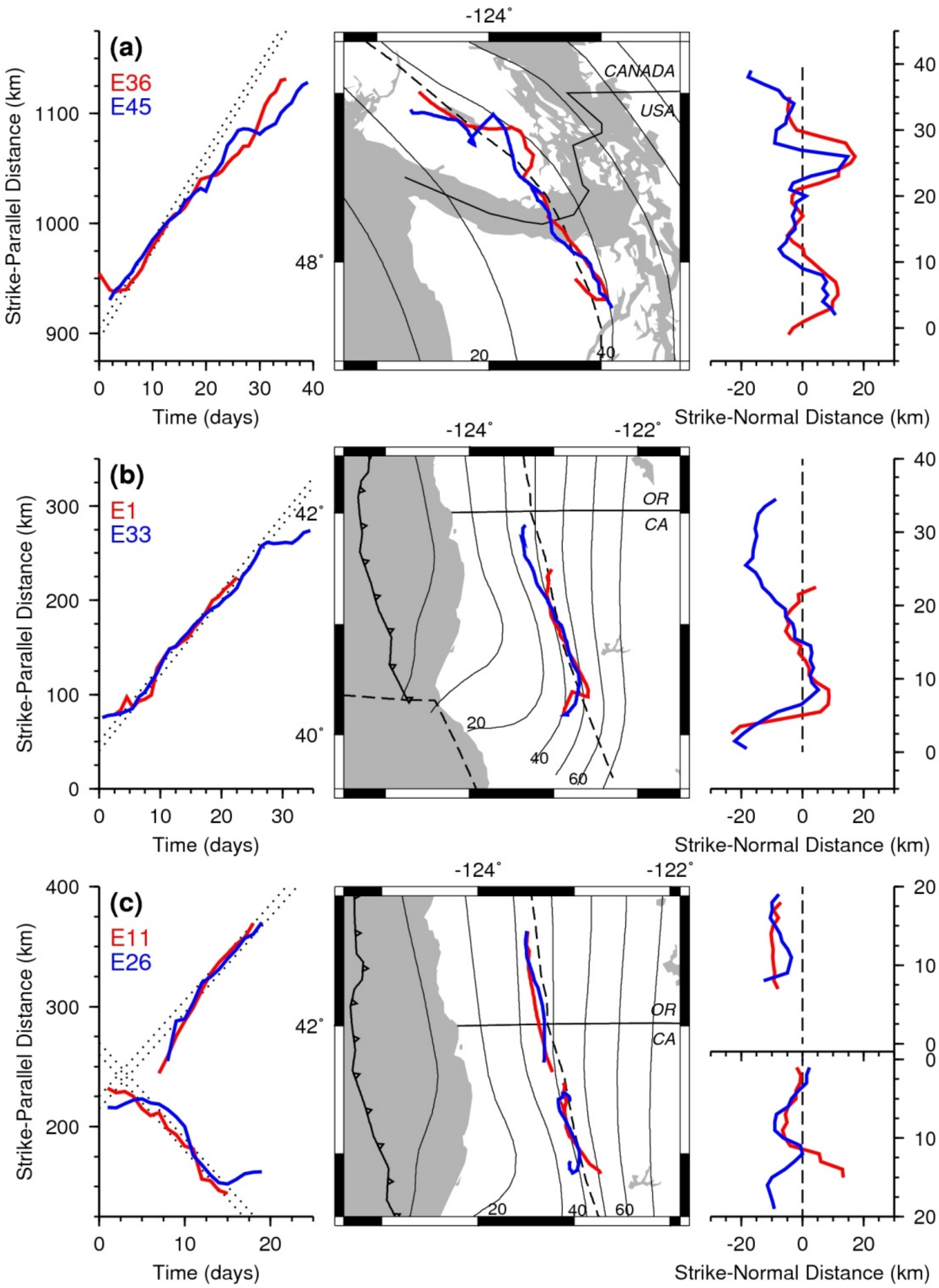


Figure 5. Pairs of episodes that demonstrate repeating migration patterns. Red indicates earlier episode, blue indicates later. Colored lines connect average daily locations showing (left) along-strike migration rate, (center) geographic migration, and (right) strike-normal migration. For reference, dotted lines show a slope of 8 km/day, separated by 10km (nominal location error). Dashed line is the overall centroid of all tremor source locations in the catalog. Thin solid lines indicate surface of the subducting plate [McCrory et al., 2012]. Pairs in (a) northern and (b,c) southern Cascadia show similarities in geographic extent, changing migration rate, and strike-normal departures. When differences do occur, they seem to involve different strike-normal pathways at the end of an episode.

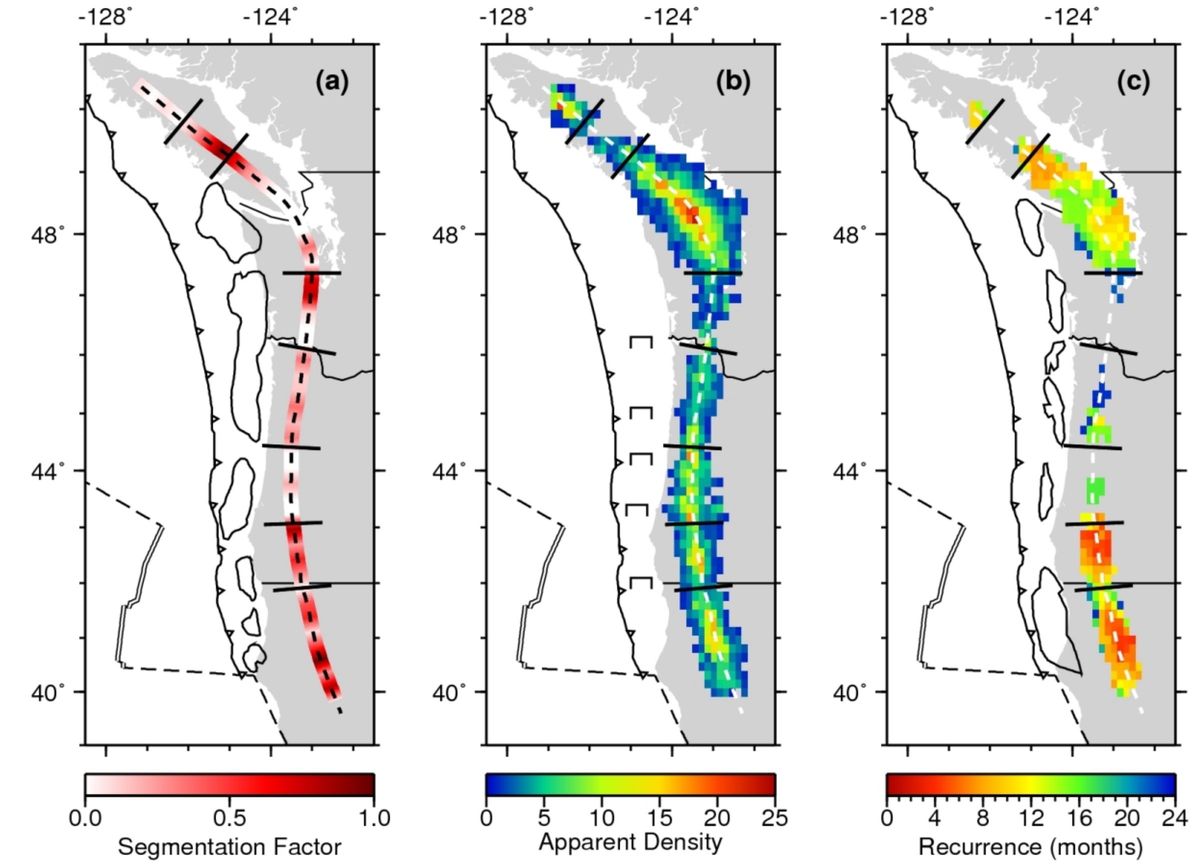


Figure 6. Evidence for segmentation of the tremor source region. (a) Tremor episode segmentation factor. Black curves are offshore gravity anomalies thought to represent megathrust asperities [Wells et al., 2003]. Red color scale indicates smoothed segmentation factor, based on cumulative tremor episode sizes that initiated or terminated at that location. Black solid lines on all three panels mark the apparent start and stop locations from visual inspection of tremor episodes (Fig. 2). (b) Tremor density per episode based on gridding of all tremor epicenters in our catalog. Black solid lines are shown again to highlight less tremor activity at apparent locations of segmentation. Offshore markers are approximate northern extent of various megathrust ruptures based on paleoseismic evidence [Goldfinger et al., 2012]. (c) Recurrence interval of tremor activity based on average time between episodes in 15 x 15 km bins. Black curves are offshore sedimentary basins (from north to south: Olympic, Willapa, Astoria, Newport, Coos Bay, and Eel River basins), which are thought to represent megathrust asperities [Wells et al., 2003].

Table S1 - Summary of Tectonic Tremor Episodes

| Episode | Start Date (mm/dd/yy) | Duration (days) | Length (km) | Region | Propagation Direction | Propagation Rate (km/d) | Slow Slip Reference |
|---|---|---|---|---|---|---|---|
| E1 | 09/01/05 | 21 | 193 | S1 | N | 8.8 | c |
| E2 | 09/02/05 | 26 | 270 | S6-S7 | N | 6.8-14.8 | b,d,e |
| E3 | 09/13/05 | 2 | 19 | S8 | - | - | - |
| E4 | 11/22/05 | 17 | 127 | S4 | N | 9.3 | - |
| E5 | 01/03/06 | 9 | 56 | S5 | - | - | - |
| E6 | 05/14/06 | 4 | 78 | S1 | - | - | - |
| E7 | 05/15/06 | 6 | 53 | S2 | - | - | - |
| E8 | 05/15/06 | 20 | 152 | S1 | N | 7.8 | - |
| E9 | 05/19/06 | 3 | 23 | S7 | - | - | - |
| E10 | 06/05/06 | 8 | 31 | S2 | - | - | - |
| E11 | 07/29/06 | 17 | 259 | S1-S2 | N,S | 6.8-12.0 | - |
| E12 | 09/06/06 | 6 | 60 | S8 | S | 13.6 | - |
| E13 | 10/28/06 | 3 | 19 | S2 | - | - | - |
| E14 | 10/31/06 | 6 | 53 | S1 | S | 8.3 | - |
| E15 | 11/09/06 | 5 | 65 | S6-S7 | - | - | a |
| E16 | 01/15/07 | 19 | 323 | S5-S7 | N | 11.2 | b,d,e |
| E17 | 01/23/07 | 3 | 33 | S1 | - | - | - |
| E18 | 01/27/07 | 7 | 55 | S4 | - | - | - |
| E19 | 02/09/07 | 16 | 124 | S1 | N | 8 | - |
| E20 | 02/24/07 | 2 | 18 | S1 | - | - | - |
| E21 | 02/27/07 | 5 | 41 | S8 | - | - | - |
| E22 | 05/10/07 | 8 | 82 | S2 | - | - | - |
| E23 | 06/11/07 | 21 | 118 | S4-S5 | S | 3.3-5.2 | - |
| E24 | 06/25/07 | 24 | 155 | S2-S3 | S | 5.7 | e |
| E25 | 06/29/07 | 10 | 68 | S1 | S | 8.8 | - |
| E26 | 07/17/07 | 18 | 258 | S1-S2 | N,S | 7.8-10.4 | - |
| E27 | 07/20/07 | 7 | 56 | S1 | S | 7.3 | - |
| E28 | 10/03/07 | 9 | 123 | S6-S7 | S | 15.7 | - |
| E29 | 10/11/07 | 5 | 67 | S6 | - | - | - |
| E30 | 03/09/08 | 4 | 58 | S1 | - | - | - |
| E31 | 03/21/08 | 3 | 13 | S2 | - | - | - |
| E32 | 03/30/08 | 6 | 48 | S8 | - | - | - |
| E33 | 04/03/08 | 34 | 220 | S1-S2 | N | 7.7 | - |
| E34 | 04/15/08 | 4 | 18 | S2 | - | - | - |
| E35 | 04/22/08 | 6 | 55 | S2-S3 | - | - | b,d,e |
| E36 | 04/29/08 | 36 | 274 | S6-S7 | N | 6.7-13.8 | - |
| E37 | 04/30/08 | 3 | 14 | S2 | - | - | - |
| E38 | 05/20/08 | 33 | 280 | S2-S4 | S | 9 | - |
| E39 | 05/26/08 | 9 | 133 | S1-S3 | - | - | - |
| E40 | 06/27/08 | 5 | 31 | S7 | - | - | - |
| E41 | 11/30/08 | 14 | 108 | S1 | N | 10.4 | - |
| E42 | 03/01/09 | 7 | 86 | S6-S7 | S | 10.1 | - |
| E43 | 03/08/09 | 10 | 32 | S6 | - | - | - |
| E44 | 03/10/09 | 9 | 156 | S1-S2 | S | 11.2 | - |
| E45 | 05/02/09 | 38 | 253 | S5-S6 | N | 4.6-7.1 | g |
| E46 | 06/08/09 | 5 | 36 | S1 | N | 9.1 | - |
| E47 | 07/01/09 | 10 | 59 | S2-S3 | - | - | - |

| | | | | | | | |
|---|---|---|---|---|---|---|---|
| E48 | 07/25/09 | 10 | 42 | S1 | - | - | - |
| E49 | 08/07/09 | 12 | 91 | S4-S5 | S | 6.9 | f |
| E50 | 08/09/09 | 10 | 26 | S5 | - | - | f |
| E51 | 08/27/09 | 11 | 106 | S4 | S | 9.3 | f |
| E52 | 10/04/09 | 9 | 42 | S1 | - | - | - |
| E53 | 02/05/10 | 9 | 78 | S2 | - | - | - |
| E54 | 02/21/10 | 10 | 88 | S6-S7 | N | 6.5 | - |
| E55 | 03/20/10 | 3 | 20 | S1 | - | - | - |
| E56 | 03/22/10 | 5 | 38 | S3 | - | - | - |
| E57 | 08/02/10 | 2 | 15 | S6 | - | - | - |
| E58 | 08/08/10 | 34 | 272 | S5-S6 | N | 7.1 | g |
| E59 | 09/16/10 | 4 | 23 | S2 | - | - | - |
| E60 | 10/17/10 | 6 | 38 | S1 | - | - | - |
| E61 | 11/15/10 | 21 | 180 | S1-S2 | N | 8.8 | - |
| E62 | 12/10/10 | 4 | 26 | S6-S7 | - | - | - |

a: *Wang et al*. [2008]; b: *McCaffrey* [2009]; c: *Aguiar et al*. [2009]; d: *Wech et al*. [2009]; e: *Schmidt and Gao* [2010]; f: Bartlow et al. [2011]; g: Tim Melbourne [personal communication]

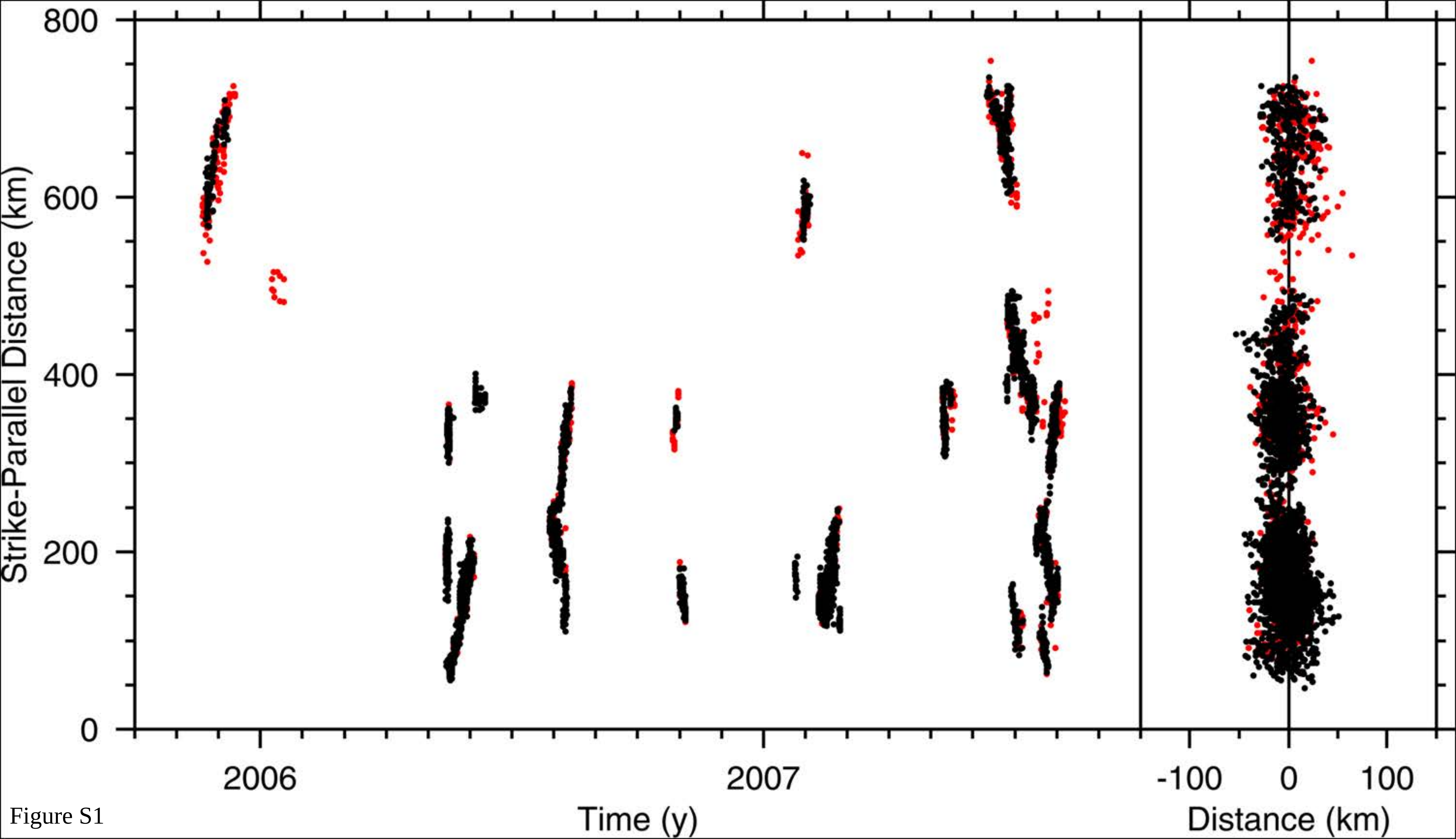

800
600
400
200
0
Strike-Parallel Distance (km)
2006
2007
Time (y)
-100
0
100
Distance (km)

Figure S1